Ab initio calculation of Kerr spectra for semi-infinite systems including multiple reflections and optical interferences

A. Vernes
Center for Computational Materials Science, Technical University Vienna, Gumpendorferstr. 1a, A-1060 Vienna, Austria

L. Szunyogh
Center for Computational Materials Science, Technical University Vienna, Gumpendorferstr. 1a, A-1060 Vienna, Austria
and Department of Theoretical Physics, Budapest University of Technology and Economics, Budafoki út 8, H-1521 Budapest, Hungary

P. Weinberger
Center for Computational Materials Science, Technical University Vienna, Gumpendorferstr. 1a, A-1060 Vienna, Austria
(Received 27 November 2001; published 4 April 2002)

Based on Luttinger's formulation the complex optical conductivity tensor is calculated within the framework of the spin-polarized relativistic screened Korringa-Kohn-Rostoker method for layered systems by means of a contour integration technique. For polar geometry and normal incidence, *ab initio* Kerr spectra of multilayer systems are then obtained by including via a 2×2 matrix technique all multiple reflections between layers and optical interferences in the layers. Applications to Co/Pt_5 and $Pt_3/Co/Pt_5$ on the top of a semi-infinite fcc(111) Pt bulk substrate show a good qualitative agreement with the experimental spectra, but differ from those obtained by applying the commonly used two-media approach.

DOI: 10.1103/PhysRevB.65.144448 PACS number(s): 75.50.Ss, 71.15.Rf, 78.20.Ls, 78.66.Bz

I. INTRODUCTION

Magneto-optical effects not only provide a powerful tool in probing the magnetic properties of solids,[1–3] but are also of direct technological interest as phenomena to be used for high-density magneto-optical recording.[2,4] Up to now, however, realistic theoretical investigations were lacking, because band-structure methods using supercells[5] cannot provide an adequate description of layered systems, for which special computational techniques such as the spin-polarized relativistic screened Korringa-Kohn-Rostoker (SKKR) method have been designed.[6–8] Furthermore, the absorptive parts of the optical conductivity tensor, as obtained from the interband contributions,[9] are not sufficient for magneto-optical Kerr spectra calculations, since the dissipative parts also have to be known. Hence, in supercell-type calculations, besides the necessity to use the Kramers-Kronig relations, one also has to include the interband contributions by means of a semiempirical Drude term.[10] Only recently a better scheme was developed by two of the present authors,[11] in which a contour integration was used to obtain the complex optical conductivity tensor as based on Luttinger's formula,[12] which in turn includes all interband and intraband contributions.[13] Combining this contour integration technique with the SKKR method, realistic interlayer and intralayer complex optical conductivities can be obtained for layered systems.

Having evaluated the interlayer and intralayer optical conductivities, the magneto-optical Kerr spectra can then be calculated by using a macroscopical model such as, e.g., the two-media approach.[14] Because a layered system contains more boundaries than just the interface between the vacuum and the surface layer, the two-media approach does not fully include the dynamics of the electromagnetic waves propagation in such systems. Since the pioneering work of Abelés in 1950,[15] several methods have been known in the literature[16,17] to treat multiple reflections and interferences using either a 2×2 matrix[18,19] or 4×4 matrix[20–22] technique. In the present paper the magneto-optical Kerr spectra of layered systems are evaluated for the most frequently used experimental setup, namely, polar geometry and normal incidence, by making use of the complex optical conductivity tensor and the 2×2 matrix technique.

In Sec. II the theoretical background is reviewed briefly. Computational aspects are then summarized in Sec. III. In Sec. IV the two-media approach (Sec. IV A) and the applied 2×2 matrix technique (Sec. IV C) are viewed as two different macroscopic models of how to calculate magneto-optical Kerr spectra of layered systems. Particular emphasis is placed in Sec. IV B on the construction of layer-resolved permittivities in terms of the (macroscopic) material equation within linear response. This construction method, combined with the 2×2 matrix technique, allows one to determine layer-resolved permittivities self-consistently, see Sec. IV C 4. As an illustration *ab initio* Kerr spectra of Co/Pt multilayer systems are presented and discussed in Sec. V. Finally, in Sec. VI the main results are summarized.

II. THEORETICAL FRAMEWORK

A. Luttinger's formalism

The frequency-dependent complex optical conductivity tensor $\tilde{\boldsymbol{\sigma}}(\omega)$ can be evaluated starting from the well-known Kubo formula and using a scalar potential description of the electric field.[23] However, by using the equivalent[24] vector potential description of the electric field, one ends up with Luttinger's formula[12]

$$\tilde{\sigma}_{\mu\nu}(\omega)=\frac{\tilde{\Sigma}_{\mu\nu}(\omega)-\tilde{\Sigma}_{\mu\nu}(0)}{\hbar\omega+i\delta}, \tag{1}$$

with the current-current correlation function as given by[25]

$$\tilde{\Sigma}_{\mu\nu}(\omega)=\frac{i\hbar}{V}\sum_{m,n}\frac{f(\epsilon_n)-f(\epsilon_m)}{\hbar\omega+i\delta+(\epsilon_n-\epsilon_m)}J^{\mu}_{nm}J^{\nu}_{mn}. \qquad (2)$$

Here $f(\epsilon)$ is the Fermi-Dirac distribution function, ϵ_m and ϵ_n are a pair of eigenvalues of the one–electron Hamiltonian, J^{μ}_{mn} are matrix elements of the electronic current operator $(\mu=x,y,z)$, and V is the reference (crystalline) volume.

The positive infinitesimal δ implies that the electromagnetic field is turned on at $t=-\infty$, and hence describes the interaction of the system with its surroundings.[26] However, as can be seen from Eq. (2), δ can also be viewed as a finite lifetime broadening, which accounts for all scattering processes at a finite temperature.

Luttinger's formula [Eq. (1)] and Eq. (2) have several advantages over the commonly used optical conductivity tensor formula of Callaway.[9] First of all, in contrast to the latter, Eq. (1) simultaneously provides both the absorptive and dissipative parts of the optical conductivity tensor. Hence there is no need for using the Kramers-Kronig relations in Luttinger's formalism. On the other hand, as recently shown,[13] Luttinger's formalism accounts for both interband and intraband contributions on the same footing. Thus by using Eq. (1) in combination with Eq. (2), one does not need to include a phenomenological Drude term in order to simulate the intraband contribution.[5] Furthermore, as was also demonstrated[13] Eqs. (1) and (2) can be used for calculations in the static $(\omega=0)$ limit, provided the lifetime broadening is kept finite $(\delta\neq 0)$.

B. Contour integration technique

Instead of evaluating the sums in the expression for the current-current correlation function [Eq. (2)] over eigenvalues of the one-electron Hamiltonian, $\tilde{\Sigma}_{\mu\nu}(\omega)$ can be calculated by means of a contour integration in the complex energy plane. For the selection of a particular contour Γ, this technique[11] exploits the facts that, with the exception of the Matsubara poles $z_k=\varepsilon_F+i(2k-1)\delta_T$ $(k=0,\pm1,\pm2,\ldots,$ and $\delta_T=\pi k_B T)$,[27] in both semiplanes the Fermi-Dirac distribution function of complex argument $f(z)$ is analytical[25] and is a real function for complex energies $z=\varepsilon\pm i\delta_j$ situated in between two successive Matsubara poles.[28] The latter property of $f(z)$, e.g., is exploited by using $\delta_j=2N_j\delta_T$, where N_1 is the number of Matsubara poles included in Γ in the upper semiplane and N_2 in the lower semiplane.[11]

By applying the residue theorem, it has been shown[11] that, equivalently to Eq. (2), one has

$$\begin{aligned}\tilde{\Sigma}_{\mu\nu}(\omega)=&\oint_{\Gamma}dz\,f(z)\,\tilde{\Sigma}_{\mu\nu}(z+\zeta,z)\\&-\left[\oint_{\Gamma}dz\,f(z)\,\tilde{\Sigma}_{\mu\nu}(z-\zeta^*,z)\right]^*\\&-2i\delta_T\sum_{k=-N_2+1}^{N_1}[\tilde{\Sigma}_{\mu\nu}(z_k+\zeta,z_k)\\&+\tilde{\Sigma}^*_{\mu\nu}(z_k-\zeta^*,z_k)],\end{aligned} \qquad (3)$$

such that

$$\tilde{\Sigma}_{\mu\nu}(0)=\oint_{\Gamma}dz\,f(z)\,\tilde{\Sigma}_{\mu\nu}(z,z)-2i\delta_T\sum_{k=-N_2+1}^{N_1}\tilde{\Sigma}_{\mu\nu}(z_k,z_k), \qquad (4)$$

where $\zeta=\hbar\omega+i\delta$ and the kernel

$$\tilde{\Sigma}_{\mu\nu}(z_1,z_2)=-\frac{\hbar}{2\pi V}\mathrm{Tr}[J^{\mu}G(z_1)\,J^{\nu}\,G(z_2)], \qquad (5)$$

is related to the electronic Green function $G(z)$. The auxiliary quantity $\tilde{\Sigma}_{\mu\nu}(z_1,z_2)$ was already used in residual resistivity calculations $(\omega,T=0)$ of substitutionally disordered bulk systems[29] and magnetotransport calculations of inhomogeneously disordered layered systems.[30] Only recently, however, it was shown,[13] that Eqs. (3)–(5) preserve all the advantages and features of Luttinger's formalism, as already mentioned above.

In the present paper, $\tilde{\Sigma}_{\mu\nu}(z_1,z_2)$ is evaluated in terms of relativistic current operators[30] and the Green functions provided by the spin-polarized relativistic SKKR method for layered systems[6–8]. The optical conductivity tensor of a multilayer system is then given[31] by

$$\tilde{\boldsymbol{\sigma}}(\omega)=\sum_{p=1}^{N}\sum_{q=1}^{N}\tilde{\boldsymbol{\sigma}}^{pq}(\omega), \qquad (6)$$

with $\tilde{\boldsymbol{\sigma}}^{pq}(\omega)$ referring to either the interlayer $(p\neq q)$ or intralayer $(p=q)$ contribution to the optical conductivity tensor.

III. COMPUTATIONAL DETAILS

In addition to the number of Matsubara poles considered, the optical conductivity tensor also depends on the number of complex energy points n_z used in order to evaluate the energy integrals in Eqs. (3) and (4), and on the number of $\vec{k}$ points used to calculate the scattering path operators that define the Green functions[7] and $\tilde{\Sigma}_{\mu\nu}(z\pm\hbar\omega+i\delta,z)$ for a given energy z. Recently, the present authors proposed two schemes to control the accuracy of these z and $\vec{k}$ integrations.[32]

The first of these schemes is meant to control the accuracy of the z integrations along each contour part by comparing the results obtained from the Konrod quadrature,[33,34] $\mathcal{K}_{2n_z+1}\tilde{\Sigma}_{\mu\nu}(\omega)$, with those from the Gauss integration rule, $\mathcal{G}_{n_z}\tilde{\Sigma}_{\mu\nu}(\omega)$.[35] On a particular part of the contour, $\tilde{\Sigma}_{\mu\nu}(\omega)$ is said to be converged if the convergence criterion[32]

$$\max|\mathcal{K}_{2n_z+1}\tilde{\Sigma}_{\mu\nu}(\omega)-\mathcal{G}_{n_z}\tilde{\Sigma}_{\mu\nu}(\omega)|\leq\varepsilon_z, \qquad (7)$$

is fulfilled for a given accuracy parameter ε_z.

The other scheme refers to the cumulative special points method,[32] which permits one to perform two-dimensional $\vec{k}$-space integrations with an arbitrary high precision. This method exploits the arbitrariness of the special points mesh origin.[36] For a given (arbitrary high) accuracy $\epsilon_{\vec{k}}$ the convergence criterion

$$\max|\mathcal{S}_{n_i}\tilde{\Sigma}_{\mu\nu}(z',z)-\mathcal{S}_{n_{i-1}}\tilde{\Sigma}_{\mu\nu}(z',z)|\leqslant\varepsilon_{\vec{k}} \tag{8}$$

has to apply for any complex energy z on the contour or z_k Matsubara pole. Here $n_i=2^{i+2}n_0$ $(n_0\in N)$ is the number of divisions along each primitive translation vector in the two-dimensional $\vec{k}$ space, and $z'=z+\zeta$ and $z-\zeta^*$.

In the present paper, the optical conductivity tensor calculations were carried out for $T=300$ K, using a lifetime broadening of 0.048 Ry and $N_2=2$ Matsubara poles in the lower semiplane. Because the computation of $\tilde{\sigma}_{\mu\nu}(\omega)$ does not depend on the form of the contour,[32] in the upper semiplane we have accelerated the calculations by considering $N_1=37$ Matsubara poles. The convergence criteria [Eqs. (7) and (8)] were fulfilled for $\varepsilon_z=\varepsilon_{\vec{k}}=10^{-3}$ a.u.

IV. MAGNETO-OPTICAL KERR EFFECT

In the case of the polar magneto-optical Kerr effect (PMOKE),[14] the Kerr rotation angle

$$\theta_K=-\frac{1}{2}(\Delta_+-\Delta_-) \tag{9}$$

and the Kerr ellipticity

$$\varepsilon_K=-\frac{r_+-r_-}{r_++r_-} \tag{10}$$

are given in terms of the complex reflectivity of the right- (+) and left-handed (–) circularly polarized light:

$$\tilde{r}_\pm=\frac{\mathcal{E}_\pm^{(\mathrm{r})}}{\mathcal{E}^{(\mathrm{i})}}=r_\pm e^{i\Delta_\pm}. \tag{11}$$

Here the complex amplitude of the reflected right- and left-handed circularly polarized light is denoted by $\mathcal{E}_\pm^{(\mathrm{r})}$, and that of the incident light by $\mathcal{E}^{(\mathrm{i})}$; $\Delta_\pm$ is the phase of the complex reflectivity $\tilde{r}_\pm$ and $r_\pm=|\tilde{r}_\pm|$. Equations (9) and (10) are exact, which can easily be deduced from simple geometrical arguments. However, in order to apply these relations, one needs to make use of a macroscopic model for the occurring reflectivities.

A. Macroscopic model I: the two-media approach

This simplest and most commonly used macroscopic model treats the multilayer system as a homogeneous, anisotropic, semi-infinite medium, such that the incident light is reflected only at the boundary between the vacuum and the surface (top) layer. In case of normal incidence the two-media approach provides an appropriate formula for the complex Kerr angle[14]

$$\tilde{\Phi}_K\equiv\theta_K-i\varepsilon_K=i\frac{\tilde{r}_+-\tilde{r}_-}{\tilde{r}_++\tilde{r}_-}, \tag{12}$$

which can be deduced from Eqs. (9) and (10) by assuming a small difference in the complex reflectivity of the right- and left-handed circularly polarized light. Because $\mathrm{Im}\,\tilde{\sigma}_{xy}(\omega)$ usually is almost a hundred times smaller than $\mathrm{Re}\,\tilde{\sigma}_{xx}(\omega)$ (see Ref. 13), the average complex refractive index of the right- and left-handed circularly polarized light is dominated by $\tilde{\sigma}_{xx}(\omega)$, and hence a direct formula results from Eq. (12),[14]

$$\tilde{\Phi}_K\approx\frac{\tilde{\sigma}_{xy}(\omega)}{\tilde{\sigma}_{xx}(\omega)}\frac{1}{\sqrt{1-\dfrac{4\pi i}{\omega}\tilde{\sigma}_{xx}(\omega)}}, \tag{13}$$

with $\tilde{\boldsymbol{\sigma}}(\omega)$ as given by Eq. (6). It should be noted that the ''direct'' formula in Eq. (13) was introduced by Reim and Schoenes[14] in order to extract the optical conductivity tensor elements $\tilde{\sigma}_{xx}(\omega)$ and $\tilde{\sigma}_{xy}(\omega)$ from experimental PMOKE data.

B. Macroscopic model II: layer-resolved permittivities

Within linear response theory[37] the Fourier-transformed macroscopic material equations,[38] averaged over the reference volume V, directly yield the total electric displacement

$$\frac{1}{V}\int_V d^3r\,\vec{D}(\vec{r},\omega)=\frac{1}{V}\int_V d^3r\int_V d^3r'\tilde{\boldsymbol{\epsilon}}(\omega;\vec{r},\vec{r}')\vec{E}(\vec{r}',\omega), \tag{14}$$

provided that the dielectric function $\tilde{\boldsymbol{\epsilon}}(\omega;\vec{r},\vec{r}')$ and the Fourier components of the electric field $\vec{E}(\vec{r}',\omega)$ are known. Using nonoverlapping cells in configuration space [the atomic sphere approximation, applied in the present approach], the reference volume can be written as

$$V=\sum_{p=1}^{N}\left(N_\parallel\sum_i\Omega_{pi}\right)\equiv\sum_{p=1}^{N}\Omega^p,$$

where $N_\parallel$ is the number of atoms per layer (the same two-dimensional lattice has to apply for each layer p), N the total number of layers, and Ω_{pi} the volume of the ith atomic sphere in layer p.

Assuming that plane waves propagate in a layer as they do in a two-dimensional unbound homogeneous medium, and that $\vec{D}_{pi}(\vec{r},\omega)=\vec{D}_p(\vec{r},\omega)$, the integral on the left-hand side of Eq. (14) can be written within the ASA as

$$\begin{aligned}\int_V d^3r\,\vec{D}(\vec{r},\omega)&\\ =N_\parallel\sum_{p=1}^{N}\vec{\mathcal{D}}_p\sum_i\Omega_{pi}&\left[1+6\sum_{k=1}^{\infty}\frac{(-1)^k(k+1)}{(2k+3)!}\right.\\ &\left.\times\left(\frac{2\pi}{\lambda_0}n_pS_{pi}\right)^{2k}\right],\end{aligned} \tag{15}$$

where $\vec{\mathcal{D}}_p$ is the amplitude of the electric displacement, $\vec{n}_p$ is the refraction vector,

$$\vec{n}_p=\frac{\vec{q}_p}{q_0}, \tag{16}$$

$\vec{q}_p$ is the wave vector ($q_0 = 2\pi/\lambda_0$ refers to the propagation constant in vacuum), and S_{pi} is the radius of the ith atomic sphere in layer p. Accordingly, the double integral on the right- hand side of Eq. (14) reduces to

$$\int_V d^3r \int_V d^3r' \tilde{\boldsymbol{\epsilon}}(\omega;\vec{r},\vec{r}')\vec{E}(\vec{r}',\omega)$$
$$= (4\pi)^2 N_{\parallel} \sum_{p,q=1}^{N} \vec{\mathcal{E}}_q \sum_{i,j} \int_0^{S_{pi}} dr\, r^2 \times \int_0^{S_{qj}} dr'\, (r')^2 \tilde{\boldsymbol{\epsilon}}^{pi,qj}(\omega;r,r') \times \left[1 + \sum_{k=1}^{\infty} \frac{(-1)^k}{(2k+1)!} \left(\frac{2\pi}{\lambda_0} n_q r'\right)^{2k}\right], \quad (17)$$

where $\vec{\mathcal{E}}_q$ is the amplitude of the electric field in layer q, and $\tilde{\boldsymbol{\epsilon}}^{pi,qj}(\omega;r,r')$ is the dielectric function $\tilde{\boldsymbol{\epsilon}}(\omega;\vec{r},\vec{r}')$ at $\vec{r} \in \Omega_{pi}$ and $\vec{r}' \in \Omega_{qj}$.

In the case of visible light the wave-vector dependence of the permittivity is negligible.[14] Therefore, after having substituted Eqs. (15) and (17) into Eq. (14), only the first term in the power series expansions has to be kept, which immediately leads to

$$\sum_{p=1}^{N} \left[\vec{\mathcal{D}}_p - \sum_{q=1}^{N} \tilde{\boldsymbol{\epsilon}}^{pq}(\omega)\vec{\mathcal{E}}_q\right] \sum_i \Omega_{pi} = 0,$$

where the interlayer ($p \neq q$), intralayer ($p = q$) permittivities are given by

$$\tilde{\boldsymbol{\epsilon}}^{pq}(\omega) = \frac{(4\pi)^2}{\sum_i \Omega_{pi}} \sum_{i,j} \int_0^{S_{pi}} dr\, r^2 \int_0^{S_{qj}} dr'\, (r')^2 \times \tilde{\boldsymbol{\epsilon}}^{pi,qj}(\omega;r,r').$$

It should be noted that a similar result connecting the static current in layer p to the electric field in layer q is already known from electric transport theory in inhomogeneous[39] or layered systems.[30] By using the relation $\vec{\mathcal{D}}_p = \tilde{\boldsymbol{\epsilon}}^{p}(\omega)\vec{\mathcal{E}}_p$, the layer-resolved permittivities $\tilde{\boldsymbol{\epsilon}}^{p}(\omega)$ are then solutions of the following system of equations:

$$\tilde{\boldsymbol{\epsilon}}^{p}(\omega)\vec{\mathcal{E}}_p = \sum_{q=1}^{N} \tilde{\boldsymbol{\epsilon}}^{pq}(\omega)\, \vec{\mathcal{E}}_q, \quad p = 1, \ldots, N. \quad (18)$$

By mapping the interlayer and intralayer contributions $\tilde{\boldsymbol{\sigma}}^{pq}(\omega)$ to the microscopically exact optical conductivity tensor $\tilde{\boldsymbol{\sigma}}(\omega)$ [Eq. (6)], onto the corresponding contributions of the permittivity tensor,

$$\tilde{\boldsymbol{\epsilon}}^{pq}(\omega) = \frac{1}{N}\left[1 + \frac{4\pi i}{\omega}\tilde{\boldsymbol{\sigma}}^{pq}(\omega)\right], \quad (19)$$

one then can establish a well-defined macroscopical model for the evaluation of Kerr spectra.

C. 2×2 matrix technique

1. Multiple reflections and optical interferences

In contrast to the two-media approach, the inclusion of all optical reflections and interferences within a multilayer system assumes that each layer acts as a homogeneous, anisotropic medium between two boundaries, and is characterized by a layer-resolved dielectric tensor $\tilde{\boldsymbol{\epsilon}}^{p}$ ($p = 1, \ldots, N$).[18,19]

As a first step the Fresnel or characteristic equation[40]

$$|\tilde{n}_p^2 \delta_{\mu\nu} - \tilde{n}_{p\mu}\tilde{n}_{p\nu} - \tilde{\epsilon}^{p}_{\mu\nu}| = 0 \quad (\mu,\nu = x,y,z) \quad (20)$$

has to be solved in order to determine the normal modes of the electromagnetic waves in a particular layer p.[41] Then by solving the Helmholtz equation for each normal mode,[41]

$$\sum_{\nu} (\tilde{n}_p^2 \delta_{\mu\nu} - \tilde{n}_{p\mu}\tilde{n}_{p\nu} - \tilde{\epsilon}^{p}_{\mu\nu})\mathcal{E}_{p\nu} = 0 \quad (\mu,\nu = x,y,z), \quad (21)$$

the corresponding $\mathcal{E}_{p\nu}$ components of the electric field in layer p are deduced. After having obtained the $\mathcal{E}_{p\nu}$s, the curl Maxwell equation[18,19]

$$\vec{\mathcal{H}}_p = \vec{n}_p \times \vec{\mathcal{E}}_p \quad (22)$$

provides the amplitudes of the magnetic fields $\vec{\mathcal{H}}_p$ for each normal mode in layer p. Here the Gaussian system of units has been used, $\vec{n}_p$ is the refraction vector, as given by Eq. (16), and $|\vec{n}_p| = \tilde{n}_p$, which in an anisotropic medium is direction and frequency dependent.[40]

Finally, the continuity of the tangential components of the electric and magnetic fields at the boundary between adjacent layers leads to a set of equations which has to be solved recursively in order to determine the magneto-optical coefficients of the layered system, such as, e.g., the surface reflectivity. If no symmetry-reduced quantities $\tilde{\boldsymbol{\epsilon}}^{p}$ are used, all the previous steps [Eqs. (20)–(22)] have to be performed numerically by using— for example— the 2×2 matrix technique of Mansuripur.[18,19]

Most frequently MOKE experiments are performed in a polar geometry using normal incidence. Therefore in the following the 2×2 matrix technique of Mansuripur is confined to this particular experimental geometry. This reduction has the advantage that, with the exception of the last step, in which the surface reflectivity has to be evaluated, all the other steps can be carried out analytically.

In the case of cubic, hexagonal or tetragonal systems and the orientation of the magnetization $\vec{M}_p$ pointing along the surface normal (z direction), the layer-resolved permittivity tensor is given by

$$\tilde{\boldsymbol{\epsilon}}^{p} = \begin{pmatrix} \tilde{\epsilon}^{p}_{xx} & \tilde{\epsilon}^{p}_{xy} & 0 \\ -\tilde{\epsilon}^{p}_{xy} & \tilde{\epsilon}^{p}_{xx} & 0 \\ 0 & 0 & \tilde{\epsilon}^{p}_{zz} \end{pmatrix}. \quad (23)$$

Assuming that $\tilde{\epsilon}^{p}_{zz} \simeq \tilde{\epsilon}^{p}_{xx}$ ($p = 1, \ldots, N$), the error introduced by this simplification— as can easily be shown — is propor-

TABLE I. Solutions of the Helmholtz equation (21) for polar geometry and normal incidence, neglecting the difference in the diagonal elements of the layer-resolved permittivity. $\mathcal{E}_{p\mu}^{(k)}$ is the amplitude of the electric field in layer p for beam k.

k	1	2	3	4
$\mathcal{E}_{px}^{(k)}$	arbitrary	$i\mathcal{E}_{py}^{(2)}$	arbitrary	$i\mathcal{E}_{py}^{(4)}$
$\mathcal{E}_{py}^{(k)}$	$i\mathcal{E}_{px}^{(1)}$	arbitrary	$i\mathcal{E}_{px}^{(3)}$	arbitrary
$\mathcal{E}_{pz}^{(k)}$	0	0	0	0

tional to the difference $\tilde{\epsilon}_{zz}^{p}-\tilde{\epsilon}_{xx}^{p}$, which in turn is usually small enough to be neglected. If in polar geometry the incidence is normal,

$$\tilde{n}_{px}=\tilde{n}_{py}=0 \quad \text{for} \quad p=1,\ldots,N,$$

the characteristic equation (20) provides four normal modes of electromagnetic waves in a layer p:

$$\tilde{n}_{pz}=\pm\sqrt{\tilde{\epsilon}_{xx}^{p}\pm i\tilde{\epsilon}_{xy}^{p}}.$$

Two of these four solutions are always situated in the lower half of the complex plane and the other two in the upper half. The first two solutions, $\tilde{n}_{pz}^{(1)}$ and $\tilde{n}_{pz}^{(2)}$ correspond to a ''downward'' (negative z direction) propagation of the electromagnetic waves, and the other two, $\tilde{n}_{pz}^{(3)}$ and $\tilde{n}_{pz}^{(4)}$, to an ''upward'' propagation (positive z direction).[18,19] These two different kinds of cases are given by

$$\tilde{n}_{pz}^{(1)}=-\sqrt{\tilde{\epsilon}_{xx}^{p}+i\tilde{\epsilon}_{xy}^{p}},$$

$$\tilde{n}_{pz}^{(2)}=-\sqrt{\tilde{\epsilon}_{xx}^{p}-i\tilde{\epsilon}_{xy}^{p}} \tag{24}$$

and

$$\tilde{n}_{pz}^{(3)}=\sqrt{\tilde{\epsilon}_{xx}^{p}+i\tilde{\epsilon}_{xy}^{p}}$$

$$\tilde{n}_{pz}^{(4)}=\sqrt{\tilde{\epsilon}_{xx}^{p}-i\tilde{\epsilon}_{xy}^{p}}. \tag{25}$$

If in a given multilayer system a particular layer p is paramagnetic, its permittivity tensor $\tilde{\boldsymbol{\epsilon}}^{p}$ is again of form shown in Eq. (23), with $\tilde{\epsilon}_{xy}^{p}=0$ and $\tilde{\epsilon}_{zz}^{p}=\tilde{\epsilon}_{xx}^{p}$. In this case only two beams are propagating, namely, those characterized by $\tilde{n}_{pz}^{(1)}\equiv\tilde{n}_{pz}^{(2)}=-\sqrt{\tilde{\epsilon}_{xx}^{p}}$ and $\tilde{n}_{pz}^{(3)}\equiv\tilde{n}_{pz}^{(4)}=\sqrt{\tilde{\epsilon}_{xx}^{p}}$. Furthermore, since the vacuum is a homogeneous, isotropic, semi-infinite medium, in addition to $\tilde{\epsilon}_{xy}=0$, $\tilde{\epsilon}_{xx}=\tilde{\epsilon}_{zz}=1$.

For each solution $\tilde{n}_{pz}^{(k)}$ $(k=1,\ldots,4)$ of the characteristic equation (20), the electric field must satisfy the Helmholtz equation (21). Because not all of the equations are independent, these can be solved only for two components of the electric field, keeping the third one arbitrary. Therefore, following the strategy proposed by Mansuripur, for beam 1 $(\tilde{n}_{pz}^{(1)})$ and beam 3 $(\tilde{n}_{pz}^{(3)})$ the corresponding $\mathcal{E}_{px}^{(k)}$ are chosen to be arbitrary, whereas for beam 2 $(\tilde{n}_{pz}^{(2)})$ and beam 4 $(\tilde{n}_{pz}^{(4)})$, the $\mathcal{E}_{py}^{(k)}$ are arbitrary.[18,19] For polar geometry and normal incidence, the solutions of the Helmholtz equation (21) are given in Table I, and the corresponding components of the magnetic field as obtained from Eq. (22) are listed in Table II.

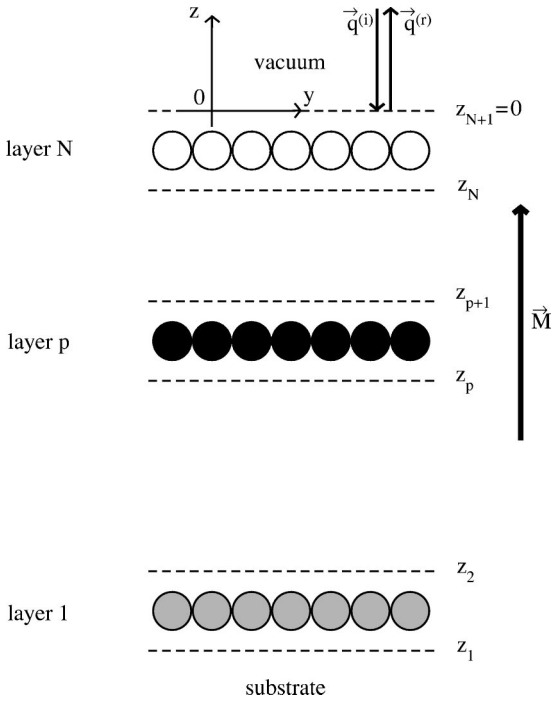

FIG. 1. The macroscopic model used for a layered system within the 2×2 matrix technique for polar geometry and normal incidence. The x axis is perpendicular to the plane of the figure, $\vec{q}^{(i)}$ is the incident wave vector and $\vec{q}^{(r)}$ is the reflected wave vector. $\vec{M}$ denotes the total spontaneous magnetization of the system.

2. Layer-resolved reflectivity matrix

Numbering the layers starting from the first one on top of the substrate toward the surface, the surface layer has the layer index $p=N$, see Fig. 1. The 2×2 reflectivity matrix $\mathcal{R}_p$ at the lower boundary z_p of layer p is given by[18,19]

$$\begin{pmatrix}\mathcal{E}_{px}^{(3)}\\ \mathcal{E}_{py}^{(4)}\end{pmatrix}=\mathcal{R}_p\begin{pmatrix}\mathcal{E}_{px}^{(1)}\\ \mathcal{E}_{py}^{(2)}\end{pmatrix}=\begin{pmatrix}\tilde{r}_p & 0\\ 0 & \tilde{r}_p'\end{pmatrix}\begin{pmatrix}\mathcal{E}_{px}^{(1)}\\ \mathcal{E}_{py}^{(2)}\end{pmatrix}; \tag{26}$$

TABLE II. Solutions of the curl Maxwell equation (22) for polar geometry and normal incidence, neglecting the difference in the diagonal elements of the layer-resolved permittivity $\boldsymbol{\epsilon}^{p}$. $\mathcal{H}_{p\mu}^{(k)}$ is the amplitude of the magnetic field in layer p for beam k.

k	1	2	3	4
$\mathcal{H}_{px}^{(k)}$	$i\mathcal{E}_{px}^{(1)}\sqrt{\tilde{\epsilon}_{xx}^{p}+i\tilde{\epsilon}_{xy}^{p}}$	$\mathcal{E}_{py}^{(2)}\sqrt{\tilde{\epsilon}_{xx}^{p}-i\tilde{\epsilon}_{xy}^{p}}$	$-i\mathcal{E}_{px}^{(3)}\sqrt{\tilde{\epsilon}_{xx}^{p}+i\tilde{\epsilon}_{xy}^{p}}$	$-\mathcal{E}_{py}^{(4)}\sqrt{\tilde{\epsilon}_{xx}^{p}-i\tilde{\epsilon}_{xy}^{p}}$
$\mathcal{H}_{py}^{(k)}$	$-\mathcal{E}_{px}^{(1)}\sqrt{\tilde{\epsilon}_{xx}^{p}+i\tilde{\epsilon}_{xy}^{p}}$	$-i\mathcal{E}_{py}^{(2)}\sqrt{\tilde{\epsilon}_{xx}^{p}-i\tilde{\epsilon}_{xy}^{p}}$	$\mathcal{E}_{px}^{(3)}\sqrt{\tilde{\epsilon}_{xx}^{p}+i\tilde{\epsilon}_{xy}^{p}}$	$i\mathcal{E}_{py}^{(4)}\sqrt{\tilde{\epsilon}_{xx}^{p}-i\tilde{\epsilon}_{xy}^{p}}$
$\mathcal{H}_{pz}^{(k)}$	0	0	0	0

also see the explicit discussion in the Appendix. The tangential components of the electric and magnetic field at a point z_p^+ just above the boundary z_p are then given by

$$\begin{pmatrix} \mathcal{E}_{px} \\ \mathcal{E}_{py} \end{pmatrix}_{z_p^+} = \mathcal{A}(\mathcal{I}+\mathcal{R}_p)\begin{pmatrix} \mathcal{E}_{px}^{(1)} \\ \mathcal{E}_{py}^{(2)} \end{pmatrix},$$

$$\begin{pmatrix} \mathcal{H}_{px} \\ \mathcal{H}_{py} \end{pmatrix}_{z_p^+} = \mathcal{B}_p^{12}(\mathcal{I}-\mathcal{R}_p)\begin{pmatrix} \mathcal{E}_{px}^{(1)} \\ \mathcal{E}_{py}^{(2)} \end{pmatrix}, \tag{27}$$

where, according to Tables I and II,

$$\mathcal{A} \equiv \begin{pmatrix} 1 & i \\ i & 1 \end{pmatrix}, \quad \mathcal{B}_p^{12} \equiv \begin{pmatrix} -i\tilde{n}_{pz}^{(1)} & -\tilde{n}_{pz}^{(2)} \\ \tilde{n}_{pz}^{(1)} & i\tilde{n}_{pz}^{(2)} \end{pmatrix} \tag{28}$$

and $\mathcal{I}$ is the 2×2 unit matrix.

Using the lower boundary z_{p-1} as a reference plane for the four beams in layer $p-1$, the tangential components of the electric and magnetic fields at a point z_p^- just below the boundary z_p are of the forms

$$\begin{pmatrix} \mathcal{E}_{px} \\ \mathcal{E}_{py} \end{pmatrix}_{z_p^-} = \mathcal{A}(\mathcal{C}_{p-1}^{12}+\mathcal{C}_{p-1}^{34}\mathcal{R}_{p-1})\begin{pmatrix} \mathcal{E}_{p-1x}^{(1)} \\ \mathcal{E}_{p-1y}^{(2)} \end{pmatrix},$$

$$\begin{pmatrix} \mathcal{H}_{px} \\ \mathcal{H}_{py} \end{pmatrix}_{z_p^-} = \mathcal{B}_{p-1}^{12}(\mathcal{C}_{p-1}^{12}-\mathcal{C}_{p-1}^{34}\mathcal{R}_{p-1})\begin{pmatrix} \mathcal{E}_{p-1x}^{(1)} \\ \mathcal{E}_{p-1y}^{(2)} \end{pmatrix}, \tag{29}$$

where

$$\mathcal{C}_{p-1}^{k,k+1} \equiv \begin{pmatrix} e^{+i\tilde{\varphi}_{p-1}^{(k)}} & 0 \\ 0 & e^{+i\tilde{\varphi}_{p-1}^{(k+1)}} \end{pmatrix}, \quad k=1,3, \tag{30}$$

with

$$\tilde{\varphi}_{p-1}^{(k)} \equiv q_0 \tilde{n}_{p-1z}^{(k)} d_{p-1}, \quad k=1,\ldots,4.$$

Here $d_p \equiv z_{p+1}-z_p$ is the thickness of layer p, $\tilde{n}_{p-1z}^{(k)}$ is defined in Eqs. (24) and (25), and q_0 is the propagation constant in vacuum, see Sec. IV B.

Based on Eqs. (27) and (29), the continuity of the tangential components of the electric and magnetic field on the boundary z_p implies that

$$(\mathcal{I}+\mathcal{R}_p)\begin{pmatrix} \mathcal{E}_{px}^{(1)} \\ \mathcal{E}_{py}^{(2)} \end{pmatrix} = (\mathcal{C}_{p-1}^{12}+\mathcal{C}_{p-1}^{34}\mathcal{R}_{p-1})\begin{pmatrix} \mathcal{E}_{p-1x}^{(1)} \\ \mathcal{E}_{p-1y}^{(2)} \end{pmatrix},$$

$$\mathcal{B}_p^{12}(\mathcal{I}-\mathcal{R}_p)\begin{pmatrix} \mathcal{E}_{px}^{(1)} \\ \mathcal{E}_{py}^{(2)} \end{pmatrix} = \mathcal{B}_{p-1}^{12}(\mathcal{C}_{p-1}^{12}-\mathcal{C}_{p-1}^{34}\mathcal{R}_{p-1})\begin{pmatrix} \mathcal{E}_{p-1x}^{(1)} \\ \mathcal{E}_{p-1y}^{(2)} \end{pmatrix},$$

such that by eliminating the electric field vectors, one immediately obtains

$$\mathcal{D}_{p-1}(\mathcal{I}+\mathcal{R}_p) = \mathcal{B}_p^{12}(\mathcal{I}-\mathcal{R}_p),$$

where

$$\mathcal{D}_{p-1} \equiv \mathcal{B}_{p-1}^{12}(\mathcal{C}_{p-1}^{12}-\mathcal{C}_{p-1}^{34}\mathcal{R}_{p-1})(\mathcal{C}_{p-1}^{12}+\mathcal{C}_{p-1}^{34}\mathcal{R}_{p-1})^{-1}. \tag{31}$$

$\mathcal{R}_p$ is therefore given in terms of $\mathcal{R}_{p-1}$ by the following simple recursion relation:

$$\mathcal{R}_p = (\mathcal{B}_p^{12}+\mathcal{D}_{p-1})^{-1}(\mathcal{B}_p^{12}-\mathcal{D}_{p-1}) \quad p=1,\ldots,N. \tag{32}$$

In order to determine the reflectivity matrix $\mathcal{R}_N$ of the surface layer, one has to evaluate all reflectivity matrices $\mathcal{R}_p$ for all layers below the surface layer. This requires starting the iterative procedure at the first layer ($p=1$) on top of the substrate. But in order to calculate $\mathcal{R}_1$, one needs to know the 2×2 matrix $\mathcal{D}_0$ corresponding to the substrate; see Eq. (32). This in turn, according to Eq. (31) is only the case if the reflectivity matrix $\mathcal{R}_0$ of the substrate is available. In order to achieve this, one has to formulate the tangential components of the electric and magnetic fields at z_1^- by taking into account that the substrate is a semi-infinite bulk without any boundaries, and hence $\mathcal{R}_0=0$.[18,19] Thus $\mathcal{D}_0=\mathcal{B}_0^{12}$, which according to Eq. (28) requires specifying the permittivity of the substrate.

3. Surface reflectivity matrix

In the vacuum region, since $\tilde{\epsilon}_{xx}=1$ and $\tilde{\epsilon}_{xy}=0$, one has to deal with the superposition of only two beams, namely, that of the incident and reflected electromagnetic waves. These beams are related through the surface reflectivity matrix $R_{\rm surf}$ such that for polar geometry and normal incidence,

$$\begin{pmatrix} \mathcal{E}_{\rm vac,x}^{\rm (r)} \\ \mathcal{E}_{\rm vac,y}^{\rm (r)} \end{pmatrix} = R_{\rm surf}\begin{pmatrix} \mathcal{E}_{\rm vac,x}^{\rm (i)} \\ \mathcal{E}_{\rm vac,y}^{\rm (i)} \end{pmatrix} \equiv \begin{pmatrix} \tilde{r}_{xx} & \tilde{r}_{xy} \\ -\tilde{r}_{xy} & \tilde{r}_{xx} \end{pmatrix}\begin{pmatrix} \mathcal{E}_{\rm vac,x}^{\rm (i)} \\ \mathcal{E}_{\rm vac,y}^{\rm (i)} \end{pmatrix}; \tag{33}$$

see the Appendix. Thus the tangential components of the electric and magnetic fields at a point z_{N+1}^+, namely, just above the interface between the vacuum and the surface, are given by

$$\begin{pmatrix} \mathcal{E}_{\rm vac,x} \\ \mathcal{E}_{\rm vac,y} \end{pmatrix}_{z_{N+1}^+} = (\mathcal{I}+R_{\rm surf})\begin{pmatrix} \mathcal{E}_{\rm vac,x}^{\rm (i)} \\ \mathcal{E}_{\rm vac,y}^{\rm (i)} \end{pmatrix},$$

$$\begin{pmatrix} \mathcal{H}_{\rm vac,x} \\ \mathcal{H}_{\rm vac,y} \end{pmatrix}_{z_{N+1}^+} = (B_{\rm vac}^{12}+B_{\rm vac}^{34}R_{\rm surf})\begin{pmatrix} \mathcal{E}_{\rm vac,x}^{\rm (i)} \\ \mathcal{E}_{\rm vac,y}^{\rm (i)} \end{pmatrix}, \tag{34}$$

where

$$B_{\rm vac}^{12} = \begin{pmatrix} 0 & 1 \\ -1 & 0 \end{pmatrix} \quad \text{and} \quad B_{\rm vac}^{34} = \begin{pmatrix} 0 & -1 \\ 1 & 0 \end{pmatrix}. \tag{35}$$

According to Eqs. (29) and (34), the continuity of the tangential components of the electric and magnetic fields at the vacuum and surface layer interface, $z_{N+1}=0$, can be written as

$$(\mathcal{I}+R_{\rm surf})\begin{pmatrix} \mathcal{E}_{\rm vac,x}^{\rm (i)} \\ \mathcal{E}_{\rm vac,y}^{\rm (i)} \end{pmatrix} = \mathcal{A}(\mathcal{C}_N^{12}+\mathcal{C}_N^{34}\mathcal{R}_N)\begin{pmatrix} \mathcal{E}_{Nx}^{(1)} \\ \mathcal{E}_{Ny}^{(2)} \end{pmatrix}$$

$$(B^{12}_{\rm vac}+B^{34}_{\rm vac}R_{\rm surf})\begin{pmatrix}\mathcal{E}^{\rm (i)}_{{\rm vac},x}\\ \mathcal{E}^{\rm (i)}_{{\rm vac},y}\end{pmatrix}=\mathcal{B}^{12}_N(\mathcal{C}^{12}_N-\mathcal{C}^{34}_N\mathcal{R}_N)\begin{pmatrix}\mathcal{E}^{(1)}_{Nx}\\ \mathcal{E}^{(2)}_{Ny}\end{pmatrix}.$$

By eliminating the electric field vectors from this system of equations, it follows that

$$\mathcal{F}_N(\mathcal{I}+R_{\rm surf})=B^{12}_{\rm vac}+B^{34}_{\rm vac}R_{\rm surf},$$

where

$$\mathcal{F}_N\equiv\mathcal{B}^{12}_N(\mathcal{C}^{12}_N-\mathcal{C}^{34}_N\mathcal{R}_N)(\mathcal{C}^{12}_N+\mathcal{C}^{34}_N\mathcal{R}_N)^{-1}\mathcal{A}^{-1}=\mathcal{D}_N\mathcal{A}^{-1}. \tag{36}$$

Thus for the surface reflectivity matrix one obtains

$$R_{\rm surf}=(\mathcal{F}_N-B^{34}_{\rm vac})^{-1}(B^{12}_{\rm vac}-\mathcal{F}_N). \tag{37}$$

The surface reflectivity matrix $R_{\rm surf}$ is therefore of the form given in Eq. (33), also see the Appendix. In spherical coordinates, one immediately obtains the complex reflectivity of the right- and left-handed circularly polarized light as

$$\tilde{r}_{\pm}=\tilde{r}_{xx}\mp i\tilde{r}_{xy},$$

which in turn determines the Kerr rotation angle θ_K and the ellipticity ϵ_K; see Eqs. (9) and (10).

4. Self-consistent layer-resolved permittivities

In order to calculate the corresponding dielectric tensor [Eq. (23)] from the interlayer and intralayer permittivities defined in Eq. (19), for a homogeneous, anisotropic layer p, a linear system of equations

$$\begin{pmatrix}\tilde{\epsilon}^p_{xx} & \tilde{\epsilon}^p_{xy}\\ -\tilde{\epsilon}^p_{xy} & \tilde{\epsilon}^p_{xx}\end{pmatrix}\begin{pmatrix}\mathcal{E}_{px}\\ \mathcal{E}_{py}\end{pmatrix}=\sum_{q=1}^{N}\begin{pmatrix}\tilde{\epsilon}^{pq}_{xx} & \tilde{\epsilon}^{pq}_{xy}\\ -\tilde{\epsilon}^{pq}_{xy} & \tilde{\epsilon}^{pq}_{xx}\end{pmatrix}\begin{pmatrix}\mathcal{E}_{qx}\\ \mathcal{E}_{qy}\end{pmatrix}$$

has to be solved; see Eq. (18). Here for $\vec{\mathcal{E}}_p$ one can take the ansatz

$$\begin{pmatrix}\mathcal{E}_{px}\\ \mathcal{E}_{py}\end{pmatrix}\equiv\begin{pmatrix}\mathcal{E}_{px}\\ \mathcal{E}_{py}\end{pmatrix}_{z=z^+_p+(d_p/2)}=\mathcal{A}[(\mathcal{C}^{12}_p)^{1/2}+(\mathcal{C}^{34}_p)^{1/2}\mathcal{R}_p]\begin{pmatrix}\mathcal{E}^{(1)}_{px}\\ \mathcal{E}^{(2)}_{py}\end{pmatrix},$$

where, due to Eq. (30),

$$(\mathcal{C}^{k,k+1}_p)^{1/2}\equiv\begin{pmatrix}e^{+iq_0\tilde{n}^{(k)}_{pz}(d_p/2)} & 0\\ 0 & e^{+iq_0\tilde{n}^{(k+1)}_{pz}(d_p/2)}\end{pmatrix},$$

$$k=1,3.$$

By using the continuity equation of the tangential components of the electric field at the boundaries [see Eqs. (27), (29) and (34)], one then obtains the layer-resolved permittivities as a weighted sum of the interlayer and intralayer permittivities defined in Eq. (19),

$$\begin{pmatrix}\tilde{\epsilon}^p_{xx} & \tilde{\epsilon}^p_{xy}\\ -\tilde{\epsilon}^p_{xy} & \tilde{\epsilon}^p_{xx}\end{pmatrix}=\sum_{q=1}^{N}W_{pq}\tilde{\boldsymbol{\epsilon}}^{pq}, \tag{38}$$

where

$$W_{pq}=\mathcal{A}\left(\prod_{k=0}^{N-q}\mathcal{W}_{q+k}\right)\left(\prod_{k=0}^{N-p}\mathcal{W}_{p+k}\right)^{-1}\mathcal{A}^{-1}, \tag{39}$$

with

$$\mathcal{W}_{p+k}=(\mathcal{I}+\mathcal{R}_{p+k})(\mathcal{C}^{12}_{p+k}+\mathcal{C}^{34}_{p+k}\mathcal{R}_{p+k})^{-1},$$

$$k=1,\ldots,N-p$$

and

$$\mathcal{W}_p=[(\mathcal{C}^{12}_p)^{1/2}+(\mathcal{C}^{34}_p)^{1/2}\mathcal{R}_p](\mathcal{C}^{12}_p+\mathcal{C}^{34}_p\mathcal{R}_p)^{-1},\quad k=0.$$

Because the 2×2 matrices $\mathcal{W}_{p+k}$ contain $\mathcal{R}_p$, $\mathcal{C}^{12}_p$, and $\mathcal{C}^{34}_p$, which in turn depend on layer-resolved permittivities $\tilde{\epsilon}^p_{\mu\nu}(\omega)$, Eq. (38) has to be solved iteratively.

The self-consistent procedure can be started by putting all 2×2 weighting matrices W_{pq} in Eq. (39) to unity, i.e., by neglecting the phase differences of the electromagnetic waves between the lower and upper boundaries in each layer p:

$$\tilde{\epsilon}^p_{\mu\nu}(\omega)^{(0)}=\sum_{q=1}^{N}\tilde{\epsilon}^{pq}_{\mu\nu}(\omega). \tag{40}$$

These quantities $\tilde{\epsilon}^p_{\mu\nu}(\omega)^{(0)}$ can be used to calculate $\mathcal{R}^{(0)}_p$ in terms of Eqs. (31) and (32). Improved layer-resolved permittivities then follow from Eq. (38). This iterative procedure has to be repeated until the difference in the old and new layer-resolved permittivities of layer p is below a numerical threshold ϵ_p:

$$\max|\tilde{\epsilon}^p_{\mu\nu}(\omega)^{(i+1)}-\tilde{\epsilon}^p_{\mu\nu}(\omega)^{(i)}|\leqslant\varepsilon_p. \tag{41}$$

V. RESULTS AND DISCUSSIONS

From experiments is known that Pt substrates ''prefer'' an fcc(111) orientation.[42] Therefore in the present contribution, calculations for the layered systems $Co/Pt_5/Pt(111)$ and $Pt_3/Co/Pt_5/Pt(111)$ have been performed, with five Pt layers serving as buffers[43] to bulk fcc Pt. The Fermi level in Eqs. (3) and (4) is that of paramagnetic fcc Pt bulk (lattice parameter of 7.4137 a.u.), which also serves as parent lattice,[43] i.e., no layer relaxation is considered.

A. Paramagnetic fcc(111) Pt substrate

As mentioned above, in order to determine the surface reflectivity the permittivity tensor of the semi-infinite substrate has to be evaluated. As can be seen from Fig. 2, the xx element of the permittivity tensor of the fcc(111) Pt substrate shows a rather simple photon energy dependence. The real part of the permittivity $\tilde{\epsilon}_{xx}(\omega)$ has a peak around 1 eV, while the imaginary part of $\tilde{\epsilon}_{xx}(\omega)$ exhibits an almost perfect hyperbolic frequency dependence. The strong decay of $\tilde{\epsilon}_{xx}(\omega)$ for photon energies in the vicinity of the static limit ($\omega=0$) can be easily understood in terms of Eqs. (19) and (40); also see Ref. 13: for $\omega\to0$ the real part of $\tilde{\epsilon}_{xx}(\omega)$ must tend to minus infinity whereas the imaginary part has to decrease. The xy element of the permittivity tensor for fcc(111) Pt

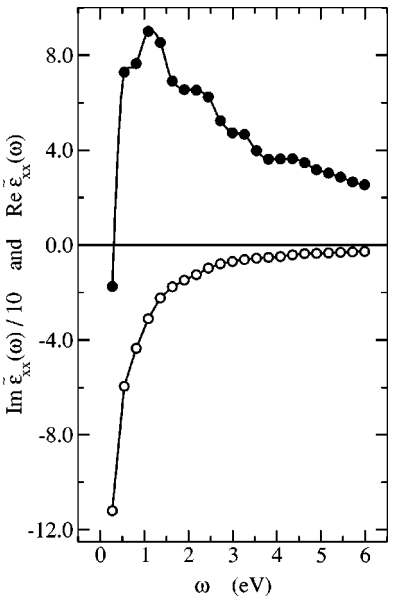

FIG. 2. The permittivity for fcc(111) Pt bulk as a function of the photon energy ω. The real part of the permittivity is denoted by full circles, and the imaginary part by open circles.

is identical zero over the whole range of optical frequencies, a functional behavior that of course does not need to be illustrated.

B. Self-consistent layer-resolved permittivities

In terms of the substrate and the zeroth-order layer-resolved permittivities, [see Eq. (40)], the iterative determination of the surface reflectivity matrix described above, also provides self-consistent, layer-resolved permittivities $\tilde{\epsilon}^{p}_{\mu\nu}(\omega)$ in a very efficient manner: in less than five iterations an accuracy of $\varepsilon_p = 10^{-13}$ for each layer p [see Eq. (41)], can be achieved. In order to illustrate this procedure, in Fig. 3 the imaginary part of the relative difference between the self-consistent and zeroth-order layer-resolved xx element of the permittivity tensor for $Co/Pt_5/Pt(111)$ with and without Pt cap layers is displayed.

This relative difference is to be viewed as the relative error made by using [according to Eq. (40)] the 2×2 matrix technique with zeroth-order layer-resolved permittivities. As can be seen from Fig. 3, this relative error is layer, frequency, and system dependent. The higher the photon energy and the larger the layered system, the less exact are the zeroth-order layer-resolved permittivities. However, for relatively small layered systems, the relative error made by using only zeroth-order permittivities is typically below 5% for $\tilde{\epsilon}_{xx}(\omega)$ and less than 20% for $\tilde{\epsilon}_{xy}(\omega)$. However, the resulting relative error in the Kerr rotation angle and the ellipticity as calculated by comparing the spectra, corresponding to the self-consistent and zeroth-order layer-resolved permittivities, is always less than 1%. Therefore, Eq. (40) can be considered as reasonably good approximation for layer-resolved permittivities.

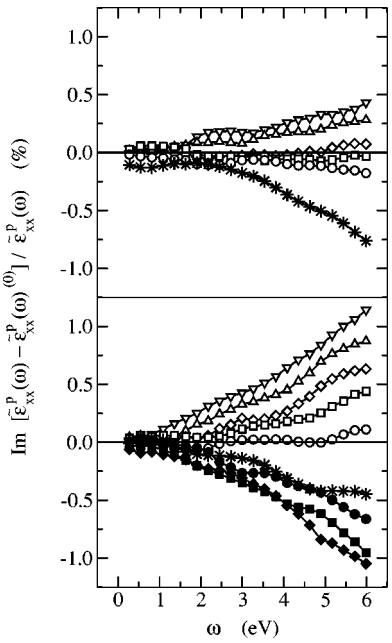

FIG. 3. Imaginary part of the relative difference between the self-consistent and zeroth-order layer-resolved xx element of the permittivity tensor as a function of the photon energy ω for fcc $Co/Pt_5/Pt(111)$ (top) and $Pt_3/Co/Pt_5/Pt(111)$ (bottom). The data represented by full (open) circles correspond to the first Pt layer on top of (under) the Co layer (stars), the squares to the second layer, and the diamonds to the third layer. Open triangles down (up) denote the first (second) Pt layer data on top of a paramagnetic fcc(111) Pt substrate.

C. Polar Kerr effect for normal incidence

The systems investigated here refer to a Co monolayer on top of a fcc(111) Pt substrate, also considering the case of three Pt cap layers. As already mentioned, five Pt layers serve as buffers to the semi-infinite host in order to ensure that the induced magnetic moments decrease monotonically to zero in the paramagnetic Pt substrate.

The *ab initio* Kerr spectra obtained from self-consistent layer-resolved permittivities, by applying the 2×2 matrix technique, are shown in Fig. 4. Usually, in experiments Pt cap layers are deposited on top of Co in order to prevent the oxidation of the surface.[44] By performing a separate, magnetic anisotropy calculation,[43] we have found that Co/Pt(111) exhibits a perpendicular magnetization only in the presence of Pt cap layers. Therefore, for the polar Kerr spectra of the $Co/Pt_5/Pt(111)$ system shown in Fig. 4 the polar geometry, namely, the perpendicular orientation of the magnetization is imposed.

Analyzing the Kerr spectra of the capped and uncapped systems in Fig. 4, several differences can be observed. The negative peak in the Kerr rotation angle θ_K at 3 eV in the spectrum of $Co/Pt_5/Pt(111)$ almost disappears from the spectrum in the case of the capped layered system. In the Kerr ellipticity the zero location at 2.8 eV, observed for the uncapped system, is shifted to 2.5 eV for the capped system, and simultaneously the infrared (IR) positive peak is shrunk and moved toward lower photon energies. Besides these features, the sign of the ultraviolet (UV) peak in both the Kerr

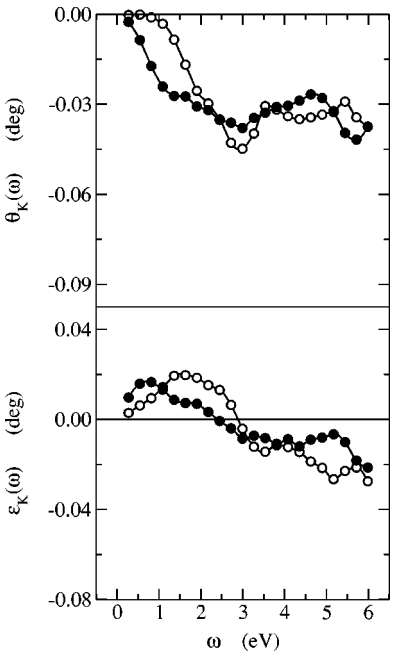

FIG. 4. The magneto-optical Kerr rotation angle $\theta_K(\omega)$ and ellipticity $\epsilon_K(\omega)$ for polar geometry and normal incidence as a function of the photon energy ω obtained by applying the 2×2 matrix technique for the self-consistent layer-resolved permittivities of fcc $Co/Pt_5/Pt(111)$ (open circles) and $Pt_3/Co/Pt_5/Pt(111)$ (full circles).

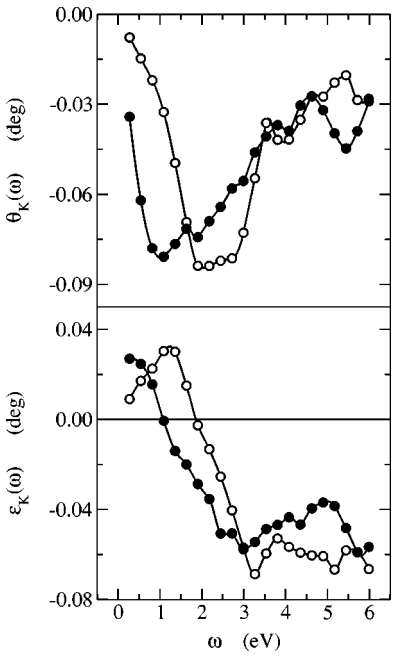

FIG. 5. As in Fig. 4, but here the Kerr spectra was obtained by applying the two-media approach for fcc $Co/Pt_5/Pt(111)$ (open circles) and $Pt_3/Co/Pt_5/Pt(111)$ (full circles).

rotation and ellipticity spectra is changed, and moves toward lower photon energies, when the Co surface layer is capped. It was found (the results are not shown here) that this shift of spectra increases with the number of Pt cap layers. These particular features can also be observed in the Kerr spectra obtained by using the two-media approach; see Fig. 5. In the two-media Kerr rotation spectrum, the negative IR peak at 2 eV in $Co/Pt_5/Pt(111)$ is shifted to about 1 eV in the case of a capped system.

Comparing the spectra in Fig. 4 with those in Fig. 5, it is evident that the theoretical Kerr spectra indeed depend on the macroscopic model used to describe the propagation of electromagnetic waves in the system. Because the systems investigated in here are much smaller than those used in experiments,[44,45] a strict quantitative comparison with experimental data cannot be made. However, a qualitative comparison based on the well-known, general features of the Co/Pt experimental Kerr spectra is still possible:[45] the Kerr rotation angle shows (a) a small negative IR peak at 1.5 eV, which decreases in amplitude with decreasing Co thickness; and (b) a high and broad negative UV peak, which moves from 4.1 to 3.9 eV for increasing Co thickness. The Kerr ellipticity is characterized by (a) a shift of the zero location at 1.5 eV (pure Co film) to 3.7 eV with decreasing Co thickness, (b) a positive peak around 3 eV, and (c) a shift of the minimum at 4.9 eV in pure Co film toward higher photon energies.

In the Kerr rotation spectra of the capped system shown in Fig. 4, there is no negative IR peak around 1.5 eV, but a negative UV exists at 5.5 eV. The Kerr ellipticity spectra of the capped system in Fig. 4 has a zero location at 2.5 eV, and positive peaks show up at 0.5, 3.5, 4, and 5 eV. These features suggest that, in the case of $Pt_3/Co/Pt_5/Pt(111)$, the Kerr spectra obtained by applying the 2×2 matrix technique are typical of Co/Pt layered systems.

A similar investigation of the Kerr rotation spectra in Fig. 5 reveals that, for the capped system, there are two negative IR peaks at 1 and 1.5 eV and a negative UV peak around 5 eV. The Kerr ellipticity for the capped system in Fig. 5 shows a zero location at 1 eV (1.5 eV in case of a pure Co film), two positive peaks at 4 and 5 eV, and a small negative peak around 3 eV. All these features make the Kerr spectra of $Pt_3/Co/Pt_5/Pt(111)$, described via the two-media approach, to resemble those of a pure Co film rather than those of a Co/Pt layered system.

Previous results, obtained by applying the 2×2 matrix technique using as substrate permittivity that of the last Pt layer below the Co one,[46] showed similar characteristics in the Kerr spectra. Hence these features cannot be ascribed to the presence of the substrate, since the substrate is taken into account in the 2×2 matrix technique, while it is not in the two-media approach. In another contribution,[31] it was shown that the optical conductivity of these systems is dominated by the contributions arising from the polarized Pt layers. Therefore, the pure Co filmlike spectra, obtained for $Pt_3/Co/Pt_5/Pt(111)$ within the two-media approach, can be seen as an indication that a layered system cannot be approximated by a homogeneous medium in which, with the exception of the reflection at the surface, no other optical reflections or interferences occur.

VI. SUMMARY

We have used the 2×2 matrix technique for the most frequently used experimental setup, namely, for polar geom-

etry and normal incidence. This technique allows one to account for all multiple reflections and optical interferences in a semi-infinite layered system. The Kerr rotation angle and ellipticity can be directly obtained from the iteratively calculated surface reflectivity matrix, which in turn can be used to determine layer-resolved permittivities self-consistently. For a free surface of layered systems, realistic *ab initio* Kerr spectra are obtained using the interlayer and intralayer conductivities as given by Luttinger's formula within the spin-polarized relativistic screened Korringa-Kohn-Rostoker method.

A comparison of the theoretical Kerr spectra of $Co/Pt_5/Pt(111)$ and $Pt_3/Co/Pt_5/Pt(111)$ as obtained by applying the 2×2 matrix technique and the two-media approach, indicates that the former technique provides typical results for layered systems, whereas the latter approach tends to generate spectra specific for homogeneous films on top of a substrate.

ACKNOWLEDGMENTS

This work was supported by the Austrian Ministry of Science (Contract No. 45.451), by the Hungarian National Science Foundation (Contract Nos. OTKA T030240 and T029813), and partially by the RTN network ''Computational Magnetoelectronics'' (Contract No. HPRN–CT–2000-00143).

APPENDIX: SYMMETRY OF REFLECTIVITY MATRICES

Since for a semi-infinite substrate, $\mathcal{R}_0=0$, $\mathcal{D}_0=\mathcal{B}_0^{12}$, with $\mathcal{B}_0^{12}$ as given by Eq. (28), according to Eq. (32), the reflectivity matrix of the first layer on top of the substrate is given by

$$\mathcal{R}_1=\begin{pmatrix}\tilde{r}_1 & 0\\ 0 & \tilde{r}_1'\end{pmatrix},$$

where

$$\tilde{r}_1=\frac{\tilde{n}_{1z}^{(1)}-\tilde{n}_{0z}^{(1)}}{\tilde{n}_{1z}^{(1)}+\tilde{n}_{0z}^{(1)}},$$

$$\tilde{r}_1'=\frac{\tilde{n}_{1z}^{(2)}-\tilde{n}_{0z}^{(2)}}{\tilde{n}_{1z}^{(2)}+\tilde{n}_{0z}^{(2)}}.$$

Assuming that all $p-1$ reflectivity matrices are of this diagonal form, namely

$$\mathcal{R}_j=\begin{pmatrix}\tilde{r}_j & 0\\ 0 & \tilde{r}_j'\end{pmatrix},\quad j=1,\ldots,(p-1),$$

by taking into account Eqs. (28) and (30), Eq. (31) immediately yields

$$\mathcal{D}_{p-1}=\begin{pmatrix}-i\tilde{d}_{p-1} & -\tilde{d}_{p-1}'\\ \tilde{d}_{p-1} & i\tilde{d}_{p-1}'\end{pmatrix},$$

where

$$\tilde{d}_{p-1}=\tilde{n}_{p-1z}^{(1)}\frac{e^{-i\tilde{\varphi}_{p-1}^{(1)}}-e^{-i\tilde{\varphi}_{p-1}^{(3)}}\tilde{r}_{p-1}}{e^{-i\tilde{\varphi}_{p-1}^{(1)}}+e^{-i\tilde{\varphi}_{p-1}^{(3)}}\tilde{r}_{p-1}},$$

$$\tilde{d}_{p-1}'=\tilde{n}_{p-1z}^{(2)}\frac{e^{-i\tilde{\varphi}_{p-1}^{(2)}}-e^{-i\tilde{\varphi}_{p-1}^{(4)}}\tilde{r}_{p-1}'}{e^{-i\tilde{\varphi}_{p-1}^{(2)}}+e^{-i\tilde{\varphi}_{p-1}^{(4)}}\tilde{r}_{p-1}'}.$$

The reflectivity matrix of layer p as obtained from the recursion relation [Eq. (32)] is also found to be diagonal,

$$\mathcal{R}_p=\begin{pmatrix}\tilde{r}_p & 0\\ 0 & \tilde{r}_p'\end{pmatrix},$$

where

$$\tilde{r}_p=\frac{\tilde{n}_{pz}^{(1)}-\tilde{d}_{p-1}}{\tilde{n}_{pz}^{(1)}+\tilde{d}_{p-1}},$$

$$\tilde{r}_p'=\frac{\tilde{n}_{pz}^{(2)}-\tilde{d}_{p-1}'}{\tilde{n}_{pz}^{(2)}-\tilde{d}_{p-1}'},$$

i.e., all the layer-resolved reflectivity matrices $\mathcal{R}_j$ ($j=1,\ldots,N$) are diagonal matrices, as anticipated in Eq. (26).

In terms of the diagonal reflectivity matrix of the surface layer $\mathcal{R}_N$, and $\mathcal{A}$ and $\mathcal{B}_N^{12}$ as given by Eq. (28), Eq. (36) reduces to

$$\mathcal{F}_N=\frac{1}{2}\begin{pmatrix}i\tilde{f}_N & -\tilde{f}_N'\\ \tilde{f}_N' & i\tilde{f}_N\end{pmatrix},$$

where

$$\tilde{f}_N=\tilde{d}_N'-\tilde{d}_N,$$

$$\tilde{f}_N'=\tilde{d}_N'+\tilde{d}_N.$$

By using $\mathcal{F}_N$, together with the matrices defined in Eq. (35), in Eq. (37), the resulting surface reflectivity matrix is of the form anticipated in Eq. (33), i.e.,

$$R_{\mathrm{surf}}=\begin{pmatrix}\tilde{r}_{xx} & \tilde{r}_{xy}\\ -\tilde{r}_{xy} & \tilde{r}_{xx}\end{pmatrix},$$

where

$$\tilde{r}_{xx}=\frac{-\tilde{f}_N^2+\tilde{f}_N'^2-4}{\tilde{f}_N^2-\tilde{f}_N'^2+4(\tilde{f}_N'-1)},$$

$$\tilde{r}_{xy}=-4i\frac{\tilde{f}_N}{\tilde{f}_N^2-\tilde{f}_N'^2+4(\tilde{f}_N'-1)}.$$

[1] W.R. Bennett, W. Schwarzacher, and W.F. Egelhoff, Phys. Rev. Lett. **65**, 3169 (1990).
[2] T.K. Hatwar, Y.S. Tyan, and C.F. Brucker, J. Appl. Phys. **81**, 3839 (1997).
[3] Y. Suzuki, T. Katayama, P.B.S. Yuasa, and E. Tamura, Phys. Rev. Lett. **80**, 5200 (1998).
[4] G.A. Bertero and R. Sinclair, J. Magn. Magn. Mater. **134**, 173 (1994).
[5] P.M. Oppeneer, T. Maurer, J. Sticht, and J. Kübler, Phys. Rev. B **45**, 10 924 (1992).
[6] L. Szunyogh, B. Újfalussy, P. Weinberger, and J. Kollár, Phys. Rev. B **49**, 2721 (1994).
[7] L. Szunyogh, B. Újfalussy, and P. Weinberger, Phys. Rev. B **51**, 9552 (1995).
[8] B. Újfalussy, L. Szunyogh, and P. Weinberger, Phys. Rev. B **51**, 12 836 (1995).
[9] J. Callaway, *Quantum Theory of the Solid State* (Academic Press, New York, 1974), Pt. B.
[10] P.M. Oppeneer, Habilitationsschrift, Technische Universität Dresden, 1999.
[11] L. Szunyogh and P. Weinberger, J. Phys.: Condens. Matter **11**, 10451 (1999).
[12] J.M. Luttinger, in *Mathematical Methods in Solid State and Superfluid Theory*, edited by R.C. Clark and G.H. Derrick (Oliver and Boyd, Edinburgh, 1967), Chap. 4, p. 157.
[13] A. Vernes, L. Szunyogh, and P. Weinberger, Phase Transit. (to be published).
[14] W. Reim and J. Schoenes, in *Magneto-optical Spectroscopy of f-electron Systems*, edited by K.H.J. Buschow and E.P. Wohlfarth (North-Holland, Amsterdam, 1990), Vol. 5, Chap. 2, p. 133.
[15] F. Abelés, Ann. Phys. (Paris) **5**, 596 (1950).
[16] D.O. Smith, Opt. Acta **12**, 13 (1965).
[17] R.P. Hunt, J. Appl. Phys. **38**, 1652 (1967).
[18] M. Mansuripur, J. Appl. Phys. **67**, 6466 (1990).
[19] M. Mansuripur, *The Principles of Magneto-Optical Recording* (Cambridge University Press, Cambridge, 1995).
[20] P. Yeh, Surf. Sci. **96**, 41 (1980).
[21] J. Zak, E.R. Moog, C. Liu, and S.D. Bader, J. Magn. Magn. Mater. **89**, 107 (1990).
[22] R. Atkinson and P.H. Lissberger, J. Magn. Magn. Mater. **118**, 271 (1993).
[23] R. Kubo, J. Phys. Soc. Jpn. **12**, 570 (1957).
[24] B.Y.-K. Hu, Am. J. Phys. **61**, 457 (1993).
[25] G.D. Mahan, *Many-Particle Physics* (Plenum Press, New York, 1990).
[26] M. Lax, Phys. Rev. **109**, 1921 (1958).
[27] D.M.C. Nicholson, G.M. Stocks, Y. Wang, W.A. Shelton, Z. Szotek, and W.M. Temmerman, Phys. Rev. B **50**, 14 686 (1994).
[28] K. Wildberger, P. Lang, R. Zeller, and P.H. Dederichs, Phys. Rev. B **52**, 11 502 (1995).
[29] W.H. Butler, Phys. Rev. B **31**, 3260 (1985).
[30] P. Weinberger, P.M. Levy, J. Banhart, L. Szunyogh, and B. Újfalussy, J. Phys.: Condens. Matter **8**, 7677 (1996).
[31] A. Vernes, L. Szunyogh, and P. Weinberger, J. Magn. Magn. Mater. **240**, 216 (2002).
[32] A. Vernes, L. Szunyogh, and P. Weinberger, J. Phys.: Condens. Matter **13**, 1529 (2001).
[33] D.P. Laurie, Math. Comput. **66**, 1133 (1997).
[34] D. Calvetti, G.H. Golub, W.B. Gragg, and L. Reichel, Math. Comput. **69**, 1035 (2000).
[35] W.H. Press, B.P. Flannery, S.A. Teukolsky, and W.T. Vetterling, *Numerical Recipes in Fortran: The Art of Scientific Computing* (Cambridge University Press, Cambridge, 1992).
[36] J. Hama and M. Watanabe, J. Phys.: Condens. Matter **4**, 4583 (1992).
[37] N.W. Ashcroft and N.D. Mermin, *Solid State Physics* (Saunders College Publishing, Fort Worth, TX, 1976).
[38] V.M. Agranovich and V.L. Ginzburg, in *Spatial Dispersion in Crystal Optics and the Theory of Excitons*, edited by R.E. Marshak, Interscience Monographs and Texts in Physics and Astronomy, Vol. XVIII (Wiley, London, 1966).
[39] W.H. Butler, X.G. Zhang, D.M.C. Nicholson, and J.M. MacLaren, J. Appl. Phys. **76**, 6808 (1994).
[40] L.D. Landau and E.M. Lifshitz, *Electrodynamics of Continuous Media*, Course of Theoretical Physics Vol. 8 (Butterworth-Heinemann, Oxford, 1999).
[41] A.K. Zvezdin and V.A. Kotov, *Modern Magnetooptics and Magnetooptical Materials*, *Studies in Condensed Matter Physics* (Institute of Physics Publishing, Bristol, 1997).
[42] D. Weller, H. Brändle, G.L. Gorman, C.J. Lin, and H. Notarys, Appl. Phys. Lett. **61**, 2726 (1992).
[43] U. Pustogowa, J. Zabloudil, C. Uiberacker, C. Blaas, P. Weinberger, L. Szunyogh, and C. Sommers, Phys. Rev. B **60**, 414 (1999).
[44] R.A. Fry, L.H. Bennett, and E.D. Torre, J. Appl. Phys. **87**, 5765 (2000).
[45] S. Uba, L. Uba, A.N. Yaresko, A.Ya. Perlov, V.N. Antonov, and R. Gontarz, Phys. Rev. B **53**, 6526 (1996).
[46] A. Vernes, L. Szunyogh, and P. Weinberger, J. Appl. Phys. (to be published).